# Thermodynamic Analysis on the Coprecipitation of Ni-Co-Mn Hydroxide

LING LI, YUNJIAO LI, LIN LI, NANXIONG CHEN, QIANG HAN, XIANZHEN ZHANG, and HU XU

The thermodynamic data of various species in Ni-$H_2O$, Co-$H_2O$, Mn-$H_2O$, and Ni-Co-Mn-$H_2O$ systems were obtained by thermodynamic calculation. The potential-pH diagrams for Ni-$H_2O$, Co-$H_2O$, and Mn-$H_2O$ systems at different ion activities at 323 K (50 °C), as well as Ni-Co-Mn-$H_2O$ complex systems at activity 1.00 at 298 K, 323 K, and 373 K (25 °C, 50 °C, and 100 °C) were constructed, respectively. The costable regions of $Ni(OH)_2$, $Co(OH)_2$, and $Mn(OH)_2$ are verified to be thermodynamically stable in aqueous solution, which indicates the thermodynamic possibility of Ni-Co-Mn hydroxide coprecipitation. The potential-pH diagrams show that the temperature and ion activity have significant effects on the coprecipitation process. As the temperature increases or the ion activity decreases, the coprecipitation region of the Ni-Co-Mn hydroxide narrows. Moreover, the metal oxides, rather than the metal hydroxide, are more easily formed when the temperature increases. Experimental confirmation was performed to further verify the constructed potential-pH diagrams. The Ni-Co-Mn hydroxide with typical hexagonal $CdI_2$ structure and quasi-spherical morphology was successfully obtained, and the SEM results show the uniform distribution of the elements Ni, Co, and Mn. The experimental results confirm the reliability of the prediction of thermodynamics analysis.

DOI: 10.1007/s11663-017-0985-x


## I. INTRODUCTION

A series of lithium cathode materials,[1] such as $LiCoO_2$, $LiNiO_2$, $LiMn_2O_4$, and $LiFePO_4$, have been widely studied to date. $LiCoO_2$[2] is believed to be the state-of-the-art cathode material due to its relative low irreversible capacity loss and good cycling performance. However, the shortage of cobalt resources and the serious pollution post a major threat to its further development. $LiNiO_2$[3] gains its popularity because of a relatively low cost and a higher reversible capacity. However, stoichiometric $LiNiO_2$ is difficult to synthesize due to the formation of lithium deficient compounds during the preparation process. In addition, it shows a poor cycle life when charged to a high voltage. $LiMn_2O_4$[4] has been extensively studied due to its low price, good thermal stability, and environmental benignity. However, the application of $LiMn_2O_4$ is greatly limited by its electrical capacitance decreasing at high temperatures, which result in decreased electrochemical stability and cycling performance. $LiFePO_4$[5] has been reported with a long working life, high safety performance, and environmental benignity. However, it also shows a low conductivity at room temperature, which has an adverse effect on large power charge-discharge. $LiNi_{1-x-y}Co_yMn_xO_2$ ($x + y < 1$, $x > 0$, and $y > 0$) has caused widespread concerns of scholars for its low-cost, stable cycling performance and safety. It has been considered as one of the most promising alternative positive materials for lithium ion batteries.

Several synthesis methods[6] have been developed to obtain $LiNi_{1-x-y}Co_yMn_xO_2$ cathode material, such as a solid-state reaction approach,[7,8] a coprecipitation process,[9,10] a sol–gel route,[11] and a spray-pyrolysis method.[12,13] As is known, the physicochemical properties and electrochemical performances of the positive materials are greatly dependent on the morphology, particle size distribution, density, *etc.* of their precursor. Therefore, a good Ni-Co-Mn hydroxide precursor is a key link in the preparation of the $LiNi_{1-x-y}Co_yMn_xO_2$ cathode material with an excellent performance. A Ni-Co-Mn hydroxide precursor with favorable spherical

LING LI, YUNJIAO LI, LIN LI, QIANG HAN, and HU XU are with the School of Metallurgy and Environment, Central South University, Changsha, Hunan, 410083, People's Republic of China, and also with Citic Dameng Mining Industries Limited, Nanning 530028, China. Contact email: yunjiao_li@csu.edu.cn NANXIONG CHEN is with Citic Dameng Mining Industries Limited. XIANZHEN ZHANG is with the School of Metallurgy and Environment, Central South University.

Manuscript submitted January 19, 2016.
Article published online August 14, 2017.

morphology is considered to be a good candidate. It can be obtained by a coprecipitation, sol–gel, or spray-pyrolysis process. However, for the sol–gel approach, a much more time-consuming technological process is necessary. As for the spray-pyrolysis route, it is difficult to realize the commercialization due to equipment limitation. Therefore, the coprecipitation method is widely considered the best choice for synthesizing a uniformly distributed, homogeneous, and phase-pure Ni-Co-Mn hydroxide precursor for $LiNi_{1-x-y}Co_yMn_xO_2$ positive material. However, to the best of the authors' knowledge, few theoretical studies on the thermodynamic analysis of the Ni-Co-Mn hydroxide coprecipitation process have been reported.

Xiao and Ye[14] and Su *et al.*[15] studied the $Me^{2+}$-$NH_3$-$OH^-$-$H_2O$ (Me = Ni, Co, Mn) coprecipitation system by thermodynamic analysis, and the lg[M]-pH graphs at different ammonia concentrations were constructed. The lg[M]-pH graphs show that every lg[M]-pH curve had an optimum pH for precipitating $Ni^{2+}$, $Co^{2+}$, and $Mn^{2+}$ at the greatest degree at a certain concentration. Hence, the process of the coprecipitation is greatly impacted by the pH and the ammonia concentration. However, it cannot reveal the exact composition of the precipitate. Though a large number of potential-pH diagrams for Ni-$H_2O$,[16,17] Co-$H_2O$,[18] and Mn-$H_2O$ systems[19,20] have been published, they are restricted to a single metal-$H_2O$ system or a specific activity value. So far, no reports on the potential-pH diagrams for Ni-Co-Mn-$H_2O$ complex systems have been found.

In this article, a series of potential-pH diagrams related to the coprecipitation of Ni-Co-Mn hydroxide were studied. The potential-pH diagrams for Ni-$H_2O$, Co-$H_2O$, and Mn-$H_2O$ simple systems at various ion activities at 323 K (50 °C), as well as Ni-Co-Mn-$H_2O$ complex systems at activity 1.00 at 298 K, 323 K, and 373 K (25 °C, 50 °C, and 100 °C) were constructed for predicting the formation of Ni-Co-Mn hydroxide. The influences of the ion activity and temperature were further discussed. $Li(Ni_{0.5}Co_{0.2}Mn_{0.3})O_2$, which has excellent electrochemical properties, was considered as one of the most potential cathode materials. Therefore, the precursor $(Ni_{0.5}Co_{0.2}Mn_{0.3})(OH)_2$ was synthesized under the guidance of the constructed potential-pH diagrams. Results from this are presented in Section IV.

## II. THERMODYNAMIC CALCULATION AND ESTIMATION

All reactions in Me-$H_2O$ systems were expressed in the following general form:

$$aA + nH^+ + ze = bB + cH_2O \qquad [1]$$

The relationship between the Gibbs free energy change of a reaction and the activities of the involved species is

$$\Delta_r G_T = \Delta_r G_T^{\Theta} + RT\ln\frac{a_{H_2O}^c a_B^b}{a_A^a a_{H^+}^n} \qquad [2]$$

where $\Delta_r G_T$ are $\Delta_r G_T^{\Theta}$ are the Gibbs free energy change of the reaction at temperature TK and the standard Gibbs free energy change of the reaction under standard condition, respectively, kJ $mol^{-1}$; $R$ represents the gas constant, J $mol^{-1}$ $K^{-1}$; $T$ is the absolute temperature, K; and $a_{H_2O}$, $a_B$, $a_A$, and$a_{H^+}$are the activities of $H_2O$, B, A, and $H^+$, respectively. $a$, $n$, $b$, and $c$ are the numbers of A, $H^+$, B, and $H_2O$ participating in the reaction.

Based on $\Delta_r G_T = -zF\varphi_T = -2.303nRT\mathrm{pH}_T$, the potential and pH for the construction of the potential-pH diagrams can be calculated by Eqs. [3] and [4], respectively:

$$\varphi_T = -\frac{\Delta_r G_T^{\Theta}}{zF} - \frac{2.303nRT}{zF}\mathrm{pH} - \frac{2.303RT}{zF}\lg\frac{a_B^b}{a_A^a} \qquad [3]$$

$$\mathrm{pH}_T = -\frac{\Delta_r G_T^{\Theta}}{2.303nRT} - \frac{b}{n}\lg a_B + \frac{a}{n}\lg a_A \qquad [4]$$

where $\varphi_T$ denotes the electrode potential of the reaction, V; $z$ is the number of the electron participating in the reaction; and $F$ refers to the Faraday constant.

The Gibbs free energy change of each reaction at elevated temperatures can be calculated from the following Equation:[21]

$$\Delta G_T^{\Theta} = \Delta G_{298}^{\Theta} - \Delta\overline{S_{298}^{\Theta}}(T-298) + \Delta\overline{C_P^{\Theta}}\left[(T-298) - T\ln\frac{T}{298}\right] \qquad [5]$$

where $\Delta G_{298}^{\Theta}$ is the standard Gibbs free change at 298 K (25 °C), $\Delta\overline{S_{298}^{\Theta}}$ is the absolute entropy value of the species, $\Delta\overline{C_P^{\Theta}}$ is the average heat capacity when temperature changes from 298 K (25 °C) to TK, $\Delta\overline{S_{298}^{\Theta}} = \Delta S_{298}^{\Theta} + 5n$, and $\Delta S_{298}^{\Theta}$ is the relative entropy value of the species.

It has been reported[22] that ignoring the contribution of the heat capacity change has little effect on the Gibbs free energy change of the reactions. Therefore, the heat capacity change in the article was neglected, so Eq. [5] is simplified as

$$\Delta G_T^{\Theta} = \Delta G_{298}^{\Theta} - \Delta\overline{S_{298}^{\Theta}}(T-298) \qquad [6]$$

For a solid compound, Latimer[23] proposed an additive method for estimating the standard entropy, in which the element value was assigned to the cation, whereas the value of the anion was variable and dependent on the cation charge.

For the aqueous oxy-anions, Connick and Powell[24] put forward Eq. [7] to calculate the entropies:

$$\Delta S_{298}^{\Theta} = 43.5 - 46(Z - 0.28n) \qquad [7]$$

where $Z$ is the absolute value of ionic charge and $n$ is the number of O atoms, excluding those included in the hydroxyl groups.

For a complex anion $MX_n^{m-n}$, the method[25] to estimate the entropies is

$$S^{\Theta}_{MX^{m-n}_n} = S^{\Theta}_{M^{m+}} + 184.933n - 168.197\frac{n}{r^{-}_{x}} \quad [8]$$

where $S^{\Theta}_{M^{m+}}$ is the entropy of the metal cation, $r^{-}_{x}$ is the radius of the anion, and the radius of the hydroxyl ion is 1.4.

In order to obtain the standard potential and $pH^{\Theta}_{T}$, the standard Gibbs free energy and standard entropy values of all the elements participating in the reactions should be obtained. The standard Gibbs free energy and standard entropy of various species considered in the Me-$H_2O$ system at 298 K (25 °C) were calculated and are given in Appendix A.

$\varphi^{\Theta}_{T}$ and $pH^{\Theta}_{T}$of all the reactions considered in the Me-$H_2O$ systems at activity 1.00 and temperatures 298 K, 323 K, and 373 K (25 °C, 50 °C, and 100 °C) were calculated using formulations [3], [4], and [6]. The results are shown in Appendices B and C.

## III. RESULTS AND DISCUSSION

The potential-pH diagrams were constructed based on the calculated data listed in Appendices B and C. The potential-pH diagrams in Me-$H_2O$ simple systems and the Ni-Co-Mn-$H_2O$ complex system are discussed in Sections III–A and III–B.

### A. *Potential-pH Diagrams in Me-$H_2O$ Simple System (Me = Ni, Co, or Mn)*

Assuming the activities of the dissolved species were 0.01, 0.10, and 1.00, the potential-pH diagrams for Ni-$H_2O$, Co-$H_2O$, and Mn-$H_2O$ simple systems at different activities at 323 K (50 °C) were constructed, as shown in Figures 1 through 3, respectively.

As shown in Figure 1, nickel occurs in various forms under different conditions in the system. $Ni^{2+}$ in aqueous solution can be converted into different solids in the form of Ni, $Ni(OH)_2$, $Ni_3O_4$, $Ni_2O_3$, or $NiO_2$ under different conditions. Especially, $Ni^{2+}$ is converted into $Ni(OH)_2$ with an increase in pH over 6.71 at activity 0.01, indicating that it is possible to synthesize $Ni(OH)_2$ by adjusting the pH value. The pH range of the stable region of $Ni(OH)_2$ ranges from 6.71 to 14.04, and the potential range is from –0.75 to 0.38 V at activity 0.01 at 323 K (50 °C). The equilibrium line between $Ni^{2+}$ and $Ni(OH)_2$ is located at pH 6.71 when the species activity is 0.01, which moves toward the negative direction to pH 5.71 at activity 1.00. However, the equilibrium line between $Ni(OH)_2$ and $HNiO_2^-$ moves from 14.04 to 16.04 when the activity changes from 0.01 to 1.00, resulting in an expansion of the region of $Ni(OH)_2$. This demonstrates that the precipitation of $Ni(OH)_2$ is more easily conducted as the species activity increases.

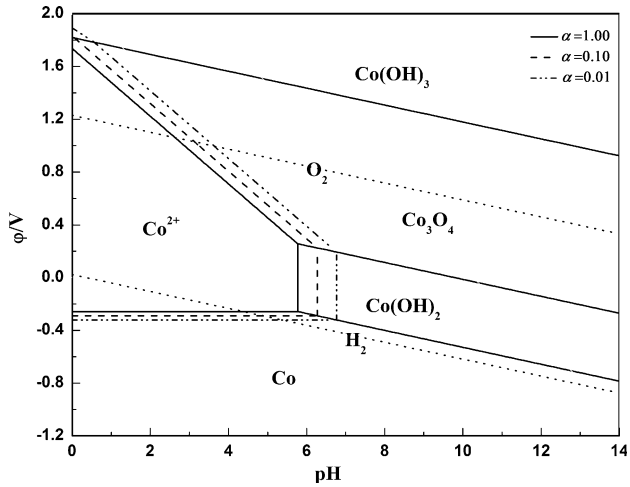


Fig. 2—Potential-pH diagram for the Co-$H_2O$ system at different activities at 323 K (50 °C).

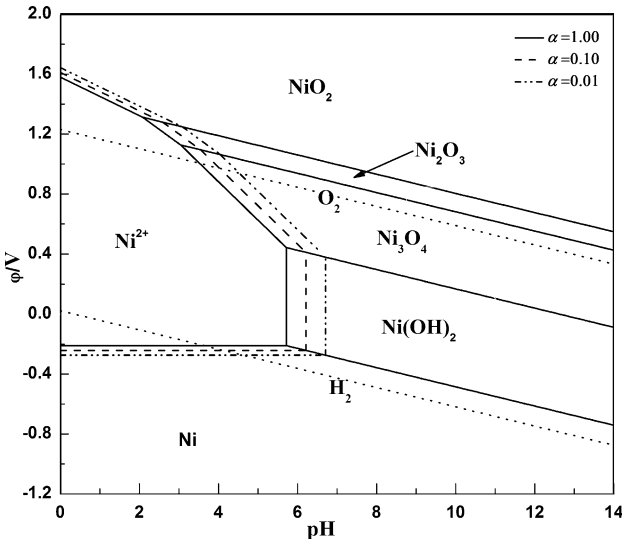


Fig. 1—Potential-pH diagram for the Ni-$H_2O$ system at different activities at 323 K (50 °C).

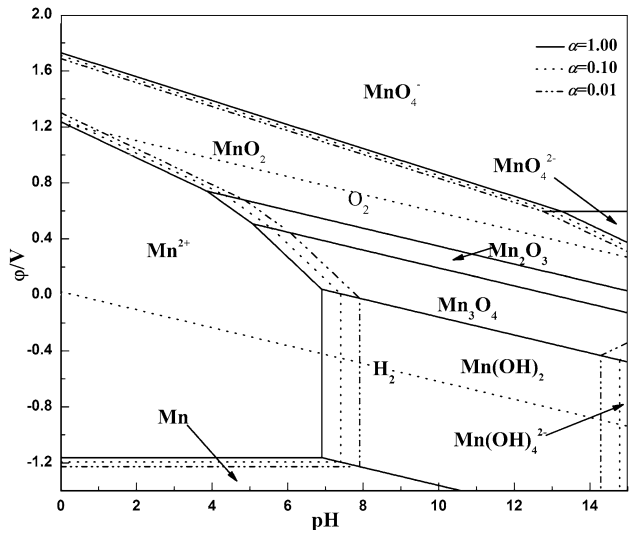


Fig. 3—Potential-pH diagram for the Mn-$H_2O$ system at different activities at 323 K (50 °C).

The Co-$H_2O$ system is similar to Ni-$H_2O$ system. As can be seen from Figure 2, $Co^{2+}$ is hydrolyzed to form $Co(OH)_2$ at pH 5.76 at activity 1.00, which is close to the precipitation pH 5.71 of $Ni(OH)_2$. The equilibrium line between $Co^{2+}$ and $Co(OH)_2$ is located at pH values 6.76 and 5.76 at activities 0.01 and 1.00, respectively. Therefore, the predominant area of $Co^{2+}$ shrinks as activity increases, resulting in the larger stability regions of the species in adjacent areas, *i.e.*, Co, $Co(OH)_2$ and $Co_3O_4$. Compared with the Ni-$H_2O$ system, the potential range of $Co(OH)_2$ is narrower than that of $Ni(OH)_2$.

Comparatively, the Mn-$H_2O$ system is more complex. $Mn^{2+}$ is transformed into $Mn(OH)_2$ at pH 6.89, which is higher than the pH values at which $Ni^{2+}$ and $Co^{2+}$ precipitate. The pH range of the predominant region of $Mn(OH)_2$ is from 6.89 to 15.28 at activity 1.00, which is smaller than both $Ni(OH)_2$ and $Co(OH)_2$. However, the potential range of $Mn(OH)_2$ is greater than those of $Ni(OH)_2$ and $Co(OH)_2$. The activity has the same effect on the predominant region of the species in the Mn-$H_2O$ system. The predominant region of $Mn^{2+}$ is minified and that of $Mn(OH)_2$ is expanded at higher activity.

From the preceding discussion, it is clear that $Ni^{2+}$, $Co^{2+}$, and $Mn^{2+}$ can be converted into $Ni(OH)_2$, $Co(OH)_2$, and $Mn(OH)_2$, respectively, under certain conditions. The stable regions of $Ni(OH)_2$, $Co(OH)_2$, and $Mn(OH)_2$ show a similar tendency as activity increases. This finding demonstrates that it is more favorable for the hydrolysis of $Me^{2+}$ to form $Me(OH)_2$ at a higher activity. However, the activity has no effect on the equilibrium lines of $Me/Me(OH)_2$ and $Me_3O_4/Me(OH)_2$.

### B. *Potential-pH Diagrams in Ni-Co-Mn-$H_2O$ Complex System*

The potential-pH diagrams for the Ni-Co-Mn-$H_2O$ complex system at activity 1.00 at 298 K, 323 K, and 373 K (25 °C, 50 °C, and 100 °C) were constructed as shown in Figures 4, 5 and 6, respectively.

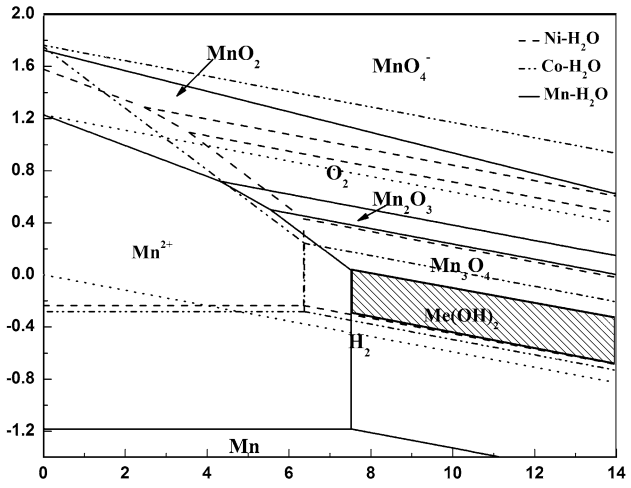


Fig. 4—Potential-pH diagram for the Ni-Co-Mn-$H_2O$ system at activity 1.00 at 298 K (25 °C).

A coprecipitation region of $Ni(OH)_2$, $Co(OH)_2$, and $Mn(OH)_2$ at 298 K (25 °C) was clearly observed in Figure 4, suggesting that the Ni-Co-Mn hydroxide can be synthesized by the coprecipitation method. The pH range of the coprecipitation region is mainly determined by $Mn(OH)_2$, which ranges from 7.51 to 16.48 at 298 K (25 °C). It moves to a lower and more favorable pH range from 5.92 to 13.35 at 373 K (100 °C), suggesting a greater possibility to obtain the coprecipitates of Ni-Co-Mn hydroxide in a weak alkaline solution at elevated temperatures. As can be seen, the top and bottom potential lines of the coprecipitation region are determined by $Mn(OH)_2$ and $Ni(OH)_2$, respectively. The equilibrium potential for $Mn(OH)_2/Mn_3O_4$ and $Mn_3O_4/Mn_2O_3$ shifts toward the negative direction with increasing temperature. Therefore, metal oxides are considered to be formed easily at a relatively high temperature. As reported in the literature,[26] the Ni-Co-Mn hydroxide precursor obtained at elevated temperature in the coprecipitation process shows a better crystallinity, but with impurity metal oxides such as $Mn_3O_4$ and $MnO_2$. The potential-pH diagrams for the Ni-Co-Mn-$H_2O$ system provide a good interpretation for the occurrence of the metal oxides.

## IV. EXPERIMENTAL CONFIRMATION

For verifying the reliability of the potential-pH diagrams, the experimental tests were conducted in two different aqueous systems: $MeSO_4$-NaOH-$H_2O$ and $MeSO_4$-NaOH-$NH_3$-$H_2O$. In the $MeSO_4$-NaOH-$H_2O$ system, a mixed aqueous solution of $NiSO_4$, $CoSO_4$, and $MnSO_4$ (all industry grade, from Changsha Deli Xitu Chemical Co., Ltd.) with Ni:Co:Mn = 5:2:3 in the molar ratio was pumped into a continuously stirred tank reactor under nitrogen atmosphere. At the same time, the NaOH solution (analytically pure, Xilong Chemical Co., Ltd.) as a precipitant was also fed into the reactor. The addition of the NaOH solution was carefully controlled to keep the pH values of the solution in the reactor constant at 9 and 10, respectively. The precipitated powders were filtered and washed with deionized water until they were without $Cl^-$ and were then dried at 393 K (120 °C).

The crystal structure of the powders was characterized by Rigaku D/max-2500 X-ray powder diffraction using $K_\alpha$ radiation. Furthermore, the morphology and composition of the particles were examined by a scanning electron microscope (SEM JEOL* JSM-6360LV) at 20 kV and inductively coupled plasma (ICP IRIS Intrepid II.XSP), respectively.

*JEOL is a trademark of Japan Electron Optics Ltd., Tokyo.

In the $MeSO_4$-NaOH-$NH_3$-$H_2O$ system, the process for obtaining the Ni-Co-Mn hydroxide precursor was similar to that in the $MeSO_4$-NaOH-$H_2O$ system. In addition, the ammonia solution (25 to 28 vol pct, Xilong Chemical Co., Ltd.) as a chelating agent was also

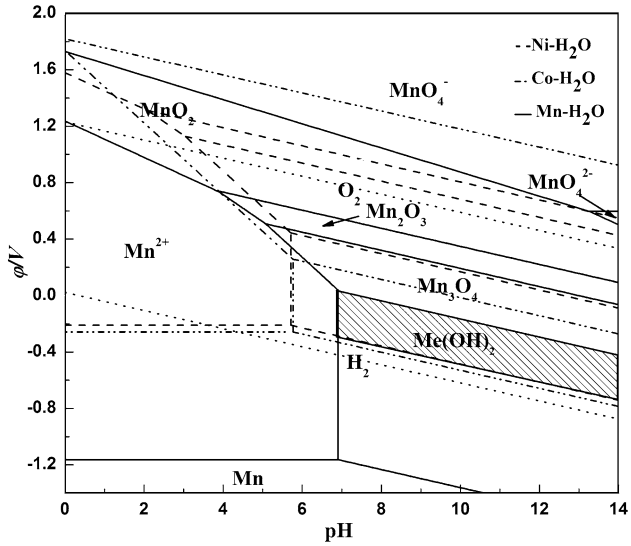


Fig. 5—Potential-pH diagram for the Ni-Co-Mn-$H_2O$ system at activity 1.00 at 323 K (50 °C).

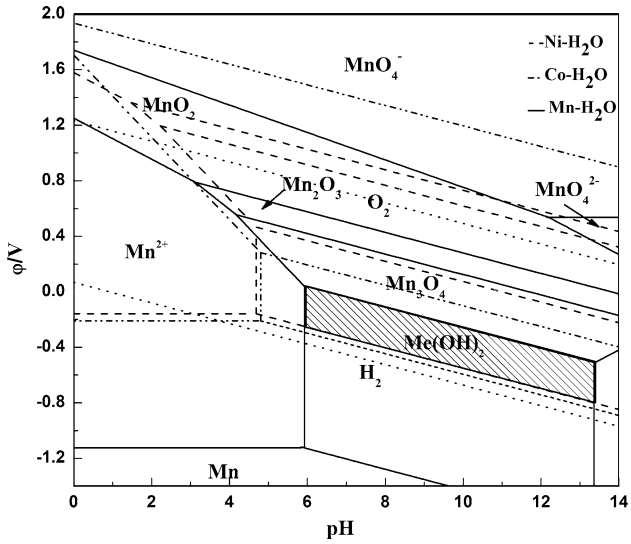


Fig. 6—Potential-pH diagram for the Ni-Co-Mn-$H_2O$ system at activity 1.00 at 373 K (50 °C).

pumped into the reactor during the precipitation process, and the pH values of the solution in the reactor were controlled at 11 and 12, respectively.

The details of the test conditions are given in Table I, and numerous experiments were performed for each sample set. Typical samples were taken for analysis. The powders, namely, A1 and A2, were prepared from the $MeSO_4$-NaOH-$H_2O$ system at pH 10 at 323 K (50 °C) and at pH 9 at 348 K (75 °C), respectively. The powders labeled N1 and N2 were obtained from the $MeSO_4$-NaOH-$NH_3$-$H_2O$ system at pH 11 and pH 12 at 323 K (50 °C), respectively.

Figure 7 shows the XRD patterns of the powders synthesized in the $MeSO_4$-NaOH-$H_2O$ system. The most intensive peak at around $2\theta = 19$ deg along with a few more characteristic peaks (100) and (101) were observed in each of the XRD patterns of these two samples. This is in good accordance with the typical $M(OH)_2$ (M = Ni, Co, Mn) structure and can be indexed to hexagonal $CdI_2$ structure. The intensity of sample A2 is stronger than that of A1, demonstrating that elevating temperature is favorable for obtaining precipitates with better crystallinity. No extra diffraction peaks related to secondary phases or impurities were detected in the patterns.

The XRD patterns of samples N1 and N2, as shown in Figure 8, can be indexed with the typical $M(OH)_2$ (M = Ni, Co, Mn) structure, which is consistent with that of A1 and A2, as given in Figure 7. The XRD patterns of the powders obtained from the systems with ammonia were slightly different from those without ammonia. Compared to Figure 7, the diffraction peaks in Figure 8 are narrower and smoother, indicating the significant effect of ammonia as a chelating agent on the crystallinity of Ni-Co-Mn hydroxide precursor.

The obtained solid samples were taken for ICP analysis to identify the contents of the metals. The results are given in Table II. As shown in Table II, the Ni:Co:Mn molar ratios of the precipitates are close to the molar ratio of Ni:Co:Mn of the feed liquid, which equals 5:2:3. Comparatively, the Ni:Co:Mn molar ratios of the samples N1 and N2 obtained from the $MeSO_4$-NaOH-$NH_3$-$H_2O$ system are closer than those of A1 and A2. The deviation of the Ni:Co:Mn molar ratios may be related to the different precipitation rates of metals, which result from the nonuniform products. It is suggested that the $MeSO_4$-NaOH-$NH_3$-$H_2O$ system is more favorable for accurately controlling the molar ratio of the metals. On the other hand, the $NH_4^+$ ion as the chelating agent in the $MeSO_4$-NaOH-$NH_3$-$H_2O$ system plays an important role in promoting the formation of the dense and sphere like hydroxide. As is well known, the sphere like hydroxide powders have been considered as an idea precursor for the production of the $LiNi_{1-x-y}Co_yMn_xO_2$ cathode materials for lithium ion batteries, and the $MeSO_4$-NaOH-$NH_3$-$H_2O$ system has been applied in industry. The contents of Ni, Co, and Mn in the mother liquid were measured, and the results show that high metal yields were obtained from both processes ($MeSO_4$-NaOH-$NH_3$-$H_2O$ and $MeSO_4$-NaOH-$H_2O$ systems).

Sample N1 with a molar ratio of Ni:Co:Mn of 4.99:2.00:3.01 was selected as the typical sample for further characterization. The SEM images of the powders of N1 are presented in Figure 9. It is obvious that the powders show similar-sphere morphology in secondary particles and the estimated particle size is about 10 to 15 $\mu$m in diameter, while the primary particles are needlelike and densely agglomerated in secondary forms.

The preceding experimental results show that Ni-Co-Mn hydroxide powders with molar ratio 5:2:3 of Ni:Co:Mn were successfully synthesized using the coprecipitation method. This is in a good agreement with the presented potential-pH diagrams.

**Table I. Test Conditions for Preparing Ni-Co-Mn Hydroxide Precursor**

| Sample | Temperature [K (°C)] | pH | Concentration of $NH_4OH$ Solution (mol/L) |
|---|---|---|---|
| A1 | 323 K (50 °C) | 10 | 0 |
| A2 | 348 K (75 °C) | 9 | 0 |
| N1 | 323 K (50 °C) | 11 | 0.5 |
| N2 | 32 K (50 °C) | 12 | 0.5 |

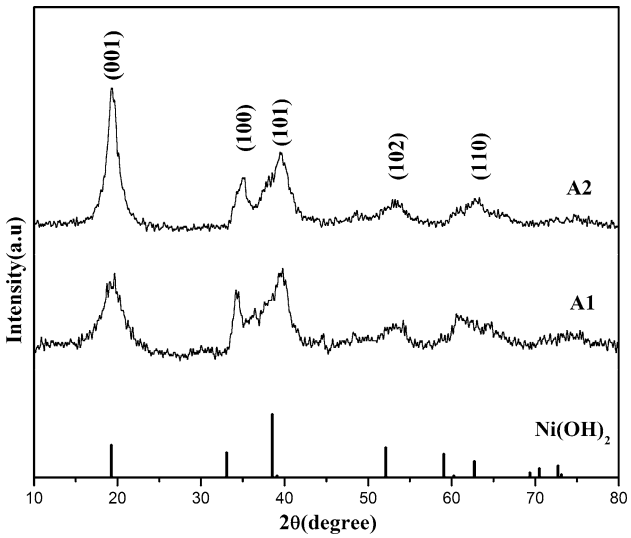


Fig. 7—XRD patterns of the powders synthesized without ammonia.

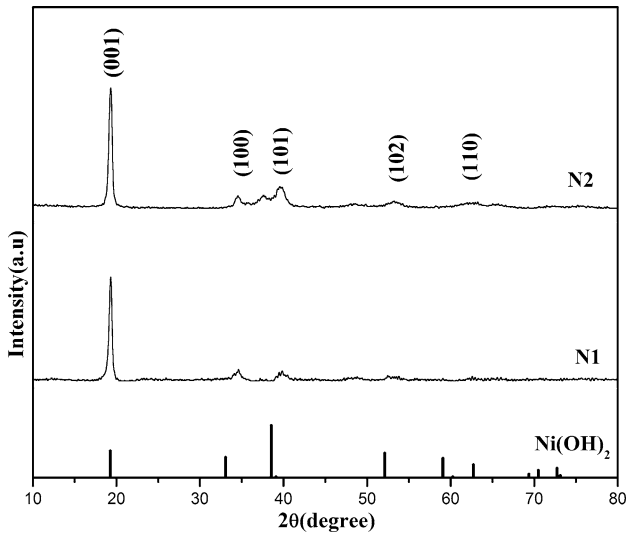


Fig. 8—XRD patterns of powders prepared at different values of pH.

## V. CONCLUSIONS

In our work, the potential-pH diagrams of Ni-$H_2O$, Co-$H_2O$, and Mn-$H_2O$ simple systems and the Ni-Co-Mn-$H_2O$ complex system were constructed. The existence of the costable area of $Ni(OH)_2$, $Co(OH)_2$, and $Mn(OH)_2$ indicates that it is possible to synthesize Ni-Co-Mn hydroxide precursor by a coprecipitation method. It is concluded that the stable region of the Ni-Co-Mn hydroxide is greatly affected by the activities of the aqueous species and the temperature. In the potential-pH diagrams, the predominant region of metal hydroxide is reduced with a decrease in ion activity and an increase in temperature. Furthermore, the formation of the metal hydroxides is easier at elevated temperatures. The Ni-Co-Mn hydroxide precursors were obtained from the two processes ($MeSO_4$-NaOH-$NH_3$-$H_2O$ and $MeSO_4$-NaOH-$H_2O$ systems) in the verified experiments under the guidance of the given potential-pH diagrams. The experimental results are good, consistent with the constructed potential-pH diagrams. It is indicated that the $MeSO_4$-NaOH-$NH_3$-$H_2O$ system is better for the production of the Ni-Co-Mn hydroxide with an accurate composition and a sphere like morphology.

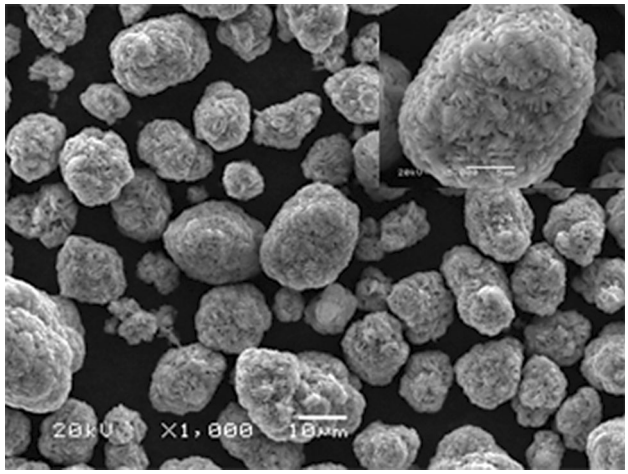


Fig. 9—SEM images of the powder N1.

**Table II. Ratios of Ni:Co:Mn of the Samples**

| Sample | w(Ni)/Pct | w(Co)/Pct | w(Mn)/Pct | Ratio of Ni:Co:Mn |
|---|---|---|---|---|
| A1 | 28.71 | 12.26 | 15.62 | 4.89:2.08:2.84 |
| A2 | 29.60 | 12.75 | 15.42 | 5.04:2.16:2.80 |
| N1 | 29.31 | 11.81 | 16.56 | 4.99:2.00:3.01 |
| N2 | 29.68 | 12.73 | 16.96 | 5.05:2.16:3.08 |

## ACKNOWLEDGMENTS

The authors are grateful for the financial support from the Government of Guangxi Zhuang Autonomous Region (Glorious Laurel Scholar Program No. 2011A025).

## APPENDIX A

See Table AI.

**Table AI. $\Delta_r G^{\Theta}_{298.15}$ and $\Delta_r S^{\Theta}_{298.15}$ of Various Species Considered in the Me-$H_2O$ System at 298.15 K (25 °C)**

| Species | $\Delta_r G^{\Theta}_{298}$ (kJ $mol^{-1}$) | $\Delta S^{\Theta}_{298}$ (J $mol^{-1}$ $K^{-1}$) |
|---|---|---|
| $Co^{2+}$ | –54.40* | –154.84* |
| $Co^{3+}$ | 134.00* | –367.76* |
| $HCoO_2^-$ | –347.15** | 62.84 |
| $H^+$ | 0.00* | –20.92* |
| $H_2O$ | –237.14* | 69.95* |
| Co | 0.00* | 30.00* |
| $Co_3O_4$ | –774.00* | 102.50* |
| $Co(OH)_2$ | –456.06† | 82.01† |
| $Co(OH)_3$ | –596.64† | 83.68† |
| $Ni^{2+}$ | –45.60* | –170.74* |
| $HNiO_2^-$ | –349.22‡ | 62.84 |
| Ni | 0.00* | 29.87 |
| $NiO_2$ | –215.14§ | 53.05§ |
| $Ni_2O_3$ | –469.74§ | 89.96§ |
| $Ni_3O_4$ | –711.91§ | 149.20§ |
| $Ni(OH)_2$ | –447.30* | 88.00§ |
| $Mn^{2+}$ | –228.10* | –115.44* |
| $MnO_4^-$ | –440.28¶ | 217.15¶ |
| $MnO_4^{2-}$ | –500.80* | 100.84* |
| $Mn(OH)_4^{2-}$ | –902.93¶¶ | 227.41 |
| Mn | 0.00* | 32.01* |
| $MnO_2$ | –465.20* | 53.10* |
| $Mn_2O_3$ | –881.20* | 110.50* |
| $Mn_3O_4$ | –1283.20* | 155.60* |
| $Mn(OH)_2$ | –616.70¶ | 81.59¶ |
| $H_2$ | 0.00* | 130.68* |
| $O_2$ | 0.00* | 205.15* |

*Speight.[27]
**Wen *et al.*[28]
†Zhong and Mei.[21]
‡Guo *et al.*[29]
§Cowan and Staehle.[30]
¶Lin *et al.*[31]
¶¶Zhao and Huo.[32]

## APPENDIX B

See Table BI.

**Table BI. $\varphi^{\Theta}_T$ of Reactions in the Me-$H_2O$ Systems at 298 K, 323 K, and 373 K (25 °C, 50 °C, and 100 °C)**

| Reactions | $\varphi^{\Theta}_T$ 298 | 323 | 373 |
|---|---|---|---|
| $Ni^{2+} + 2e = Ni$ | –0.24 | –0.21 | –0.16 |
| $Ni(OH)_2 + 2e + 2H^+ = Ni + 2H_2O$ | 0.14 | 0.15 | 0.19 |
| $HNiO_2^- + 3H^+ + 2e = Ni + 2H_2O$ | 0.65 | 0.67 | 0.71 |
| $Ni_3O_4 + 2H_2O + 2e + 2H^+ = 3Ni(OH)_2$ | 0.81 | 0.81 | 0.81 |
| $Ni_3O_4 + 2e + 8H^+ = 3Ni^{2+} + 4H_2O$ | 1.93 | 1.91 | 1.85 |
| $Ni_3O_4 + 2H_2O + 2e = 3HNiO_2^- + H^+$ | –0.72 | –0.73 | –0.76 |
| $Ni_2O_3 + 2e + 6H^+ = 2Ni^{2+} + 3H_2O$ | 1.72 | 1.71 | 1.69 |
| $3Ni_2O_3 + 2e + 2H^+ = 2Ni_3O_4 + H_2O$ | 1.30 | 1.32 | 1.36 |
| $Ni_2O_3 + H_2O + 2e = 2HNiO_2^-$ | –0.04 | –0.05 | –0.06 |
| $2NiO_2 + 2e + 2H^+ = Ni_2O_3 + H_2O$ | 1.43 | 1.44 | 1.47 |
| $NiO_2 + 2e + 4H^+ = Ni^{2+} + 2H_2O$ | 1.58 | 1.58 | 1.58 |
| $NiO_2 + 2e + H^+ = HNiO_2^-$ | 0.69 | 0.70 | 0.71 |
| $Co^{3+} + e = Co^{2+}$ | 1.95 | 2.01 | 2.12 |
| $Co^{3+} + 2H_2O + e = HCoO_2^- + 3H^+$ | 0.07 | 0.13 | 0.25 |
| $Co(OH)_2 + 2H^+ + 2e = Co + 2H_2O$ | 0.09 | 0.11 | 0.14 |
| $Co_3O_4 + 2H_2O + 2H^+ + 2e = 3Co(OH)_2$ | 0.62 | 0.63 | 0.64 |
| $3Co(OH)_3 + H^+ + e = Co_3O_4 + 5H_2O$ | 1.76 | 1.82 | 1.93 |
| $Co^{2+} + 2e = Co$ | –0.28 | –0.26 | –0.21 |
| $HCoO_2^- + 3H^+ + 2e = Co + 2H_2O$ | 0.66 | 0.68 | 0.72 |
| $Co_3O_4 + 2H_2O + 2e = 3HCoO_2^- + H^+$ | –1.07 | –1.08 | –1.10 |
| $Co_3O_4 + 8H^+ + 2e = 3Co^{2+} + 4H_2O$ | 1.75 | 1.73 | 1.70 |
| $Co(OH)_3 + 3H^+ + e = Co^{2+} + 3H_2O$ | 1.75 | 1.76 | 1.78 |
| $Co(OH)_3 + e = HCoO_2^- + H_2O$ | –0.13 | –0.11 | –0.09 |
| $Mn^{2+} + 2e = Mn$ | –1.18 | –1.16 | –1.12 |
| $MnO_2 + 4H^+ + 2e = Mn^{2+} + 2H_2O$ | 1.23 | 1.24 | 1.25 |
| $Mn(OH)_2 + 2H^+ + 2e = Mn + 2H_2O$ | –0.74 | –0.72 | –0.69 |
| $Mn(OH)_4^{2-} + 4H^+ + 2e = Mn + 4H_2O$ | 0.24 | 0.26 | 0.30 |
| $Mn_3O_4 + 2H_2O + 2H^+ + 2e = 3Mn(OH)_2$ | 0.48 | 0.48 | 0.48 |
| $Mn_3O_4 + 8H^+ + 2e = 3Mn^{2+} + 4H_2O$ | 1.81 | 1.80 | 1.79 |
| $3Mn_2O_3 + 2H^+ + 2e = 2Mn_3O_4 + H_2O$ | 0.83 | 0.84 | 0.86 |
| $Mn_3O_4 + 8H_2O + 2e = 3Mn(OH)_4^{2-} + 4H^+$ | –2.44 | –2.46 | –2.49 |
| $2MnO_2 + 2H^+ + 2e = Mn_2O_3 + H_2O$ | 0.97 | 0.99 | 1.02 |
| $Mn_2O_3 + 5H_2O + 2e = 2Mn(OH)_4^{2-} + 2H^+$ | –1.35 | –1.36 | 1.37 |
| $Mn_2O_3 + 6H^+ + 2e = 2Mn^{2+} + 3H_2O$ | 1.48 | 1.48 | 1.48 |
| $MnO_4^- + 4H^+ + 3e = MnO_2 + 2H_2O$ | 1.72 | 1.73 | 1.74 |
| $MnO_4^{2-} + 4H^+ + 2e = MnO_2 + 2H_2O$ | 2.27 | 2.30 | 2.34 |
| $MnO_4^- + e = MnO_4^{2-}$ | 0.63 | 0.60 | 0.54 |
| $MnO_2 + 2H_2O + 2e = Mn(OH)_4^{2-}$ | –0.19 | –0.18 | –0.18 |
| $MnO_4^{2-} + 4H^+ + 4e = Mn(OH)_4^{2-}$ | 1.04 | 1.05 | 1.08 |
| $2H^+ + 2e = H_2$ | 0 | 0.02 | 0.07 |
| $O_2 + 4H^+ + 4e = 2H_2O$ | 1.23 | 1.23 | 1.23 |

## APPENDIX C

See Table CI.

**Table CI. $pH_T^{\Theta}$ of Reactions in the Me-$H_2O$ Systems at 298 K, 323 K, and 373 K (25 °C, 50 °C, and 100 °C)**

| Reactions | $pH_T^{\Theta}$ | | |
|---|---|---|---|
| | 298 | 323 | 373 |
| $Ni(OH)_2 + 2H^+ = Ni^{2+} + 2H_2O$ | 6.36 | 5.71 | 4.68 |
| $HNiO_2^- + H^+ = Ni(OH)_2$ | 17.19 | 16.04 | 14.22 |
| $Co^{2+} + 2H_2O = Co(OH)_2 + 2H^+$ | 6.36 | 5.76 | 4.80 |
| $HCoO_2^- + H^+ = Co(OH)_2$ | 19.09 | 17.77 | 15.67 |
| $Co^{3+} + 3H_2O = Co(OH)_3 + 3H^+$ | –1.68 | –1.28 | –1.52 |
| $Co^{2+} + 2H_2O = HCoO_2^- + 3H^+$ | 10.60 | 9.76 | 8.42 |
| $Mn^{2+} + 2H_2O = Mn(OH)_2 + 2H^+$ | 7.51 | 6.89 | 5.92 |
| $Mn(OH)_2 + 2H_2O = Mn(OH)_4^{2-} + 2H^+$ | 16.48 | 15.28 | 13.35 |

## REFERENCES


1. M.S. Whittingham: *Am. Chem. Soc.*, 2004, vol. 104, pp. 4271–4301.
2. Y.S. Jung, A.S. Cavanagh, A.C. Dillon, M.D. Groner, S.M George, and S.H Lee: *Electrochem. Soc.*, 2010, vol. 157, pp. A75–A81.
3. Z.C Liu, H.H Zhen, Y. Kim, and C.D Liang: *Power Sources,* 2011, vol. 196, pp. 10201–20206.
4. T.F. Yi, Y.R. Zhu, X.D. Zhu, J. Shu, C.B. Yue, and A.N. Zhou: *Ionics*, 2009, vol. 15, pp. 779–84.
5. A. Kuwahara, S. Suzuki, and M. Miyayama: *Electroceramics*, 2010, vol. 24, pp. 69–75.
6. D.C Li, T. Muta, L.Q. Zhang, M. Yoshio, and H. Noguchi: *Power Sources,* 2004, vol. 132, pp. 150–55.
7. T. Ohzuku and Y. Makimura: *Chem. Lett.*, 2001, vol. 7, pp. 642–43.
8. X.Y. Jiang, Y. Sha, R. Cai, and Z. Shao: *Mater. Chem. A*, 2015, vol. 3, pp. 10536–44.
9. M.H. Lee, Y.J. Kang, S.T. Myung, and Y.K. Sun: *Electrochim. Acta*, 2004, vol. 50, pp. 939–48.
10. C. Deng, L. Liu, W. Zhou, K. Sun, and D. Sun: *Electrochim. Acta*, 2008, vol. 53, pp. 2441–47.
11. C.H. Chen, C.J. Wang, and B.J. Hwang: *Power Sources*, 2005, vol. 14, pp. 626–29.
12. M. Shui, S. Gao, J. Shu, W.D. Zheng, D. Xu, L.L. Chen, L. Feng, and Y.L. Ren: *Ionics*, 2013, vol. 19, pp. 41–46.
13. S.H. Park, C.S. Yoon, S.G. Kang, H.S. Kim, S.I. Moon, and Y.K. Sun: *Electrochim. Acta*, 2004, vol. 49, pp. 557–63.
14. X.Y. Xiao and Y.Q. Ye: *South China Univ. Technol.*, 2010, vol. 38, pp. 30–34.
15. J.T. Su, Y.C. Su, and Z.G. Lan: *Chin. Batt. Industry*, 2008, vol. 13, pp. 18–21.
16. B. Beverskog and I. Puigdomench: *Corros. Sci.*, 1997, vol. 39, pp. 969–80.
17. P.A. Brook: *Corros. Sci.*, 1972, vol. 12, pp. 297–306.
18. J. Chivot, L. Mendoza, C. Mansour, T. Pauporte, and M. Cassir: *Corros. Sci.*, 2008, vol. 50, pp. 62–64.
19. B. Messaoudi, S. Joiret, M. Keddam, and H. Takenouti: *Electrochim. Acta*, 2001, vol. 46, pp. 88–90.
20. S.L. Zhang and Z.L. Liang: *Nonferrous Met.*, 1982, vol. 34, pp. 65–67.
21. Z.Q. Zhong and G.G. Mei: *Application of Diagrams of Chemical Potential in Hydrometallurgy and Purification of Waste Water*, Central South University Press, Changsha, 1986, pp. 36–38.
22. O. Kubaschcwski and C.B. Alcock: *Metallurgical Thermochemistry*, 5th ed., Metallurgical Industry Press, Beijing, 1985, p. 222.
23. W.M. Latimer: *The Oxidation States of the Elements and Their Potentials in Aqueous Solutions*, 2nd ed., Prentice-Hall, New York, NY, 1952, pp. 359–65.
24. R.E. Connick and R.E. Powell: *Chem. Phys.*, 1953, vol. 21, pp. 2006–07.
25. K.X. Tan, Q.L. Wang, and H.S. Wang: *Rong Jin Cai Kuang Re Li Xue He Dong Li Xue*, Central South University Press, ChangSha, 2003, pp. 35–36.
26. S. Zhang, C. Deng, B.L. Fu, S.Y. Yang, and L. Ma: *Power. Technol.*, 2010, vol. 198, pp. 373–80.
27. J.G. Speight: *Lange's Handbook of Chemistry*, 16th ed., McGraw-Hill, New York, NY, 2004, pp. 1246–59.
28. S.M. Wen, Z.W. Zhao, and G.S. Huo: *Chin. Power Sources*, 2005, vol. 29, pp. 423–25.
29. C.H. Guo, Z.W. Zhao, and G.S. Huo: *Chin. J. Power Sources*, 2005, vol. 29, pp. 376–78.
30. R.L. Cowan and R.W. Staehle: *Electrochem. Soc.*, 1971, vol. 118, pp. 557–59.
31. C.X. Lin, Z.H. Bai, and Z.R. Zhang: *Handbook of Minerals and Related Thermochemical Data*, Science Press, Beijing, 1985, p. 36.
32. Z.W. Zhao and G.S. Huo: *Chin. J. Nonferrous Met.*, 2004, vol. 14, pp. 1926–33.